243071: garnet-bearing sillimanite–magnetite pelitic schist, Radiator prospect

(Aileron Province, North Australian Craton)

Kelsey, DE, Korhonen, FJ, Romano, SS and Spaggiari, CV

Location and sampling

Webb (SF 52-10), Dwarf Well (4553)

MGA Zone 52, 420098E 7534602N

WAROX site CVSWAO000007

Sampled on 15 July 2019

This sample was collected from the 493.18 – 493.33 m depth interval of diamond drillcore Webb RDD01, drilled in 2010 by Meteoric Resources NL at their Radiator prospect (Reddy, 2012), with support from the Western Australian Government's Exploration Incentive Scheme (EIS). The drillhole is located west of Lake Mackay in the Great Sandy Desert, about 75 km northeast of Kiwirrkurra community, 72 km north of Mount Webb, and 61 km south-southeast of Carnegie Bluff.

Geological context

The unit sampled is a pelitic schist within crystalline basement in the northern Aileron Province of the North Australian Craton (Hollis et al., 2013). Drillhole RDD01 targeted a coincident gravity and magnetic anomaly, and intersected mainly quartz–biotite– muscovite–garnet–magnetite–apatite±sillimanite schists, interpreted as regionally metamorphosed sedimentary rocks with variable magnetite–hematite–sulfide alteration (Reddy, 2012). The present sample was collected to constrain the *P–T* conditions of metamorphism. This sample yielded an in situ garnet Lu–Hf isochron date of 1670 ± 36 Ma (n = 52) and in situ biotite Rb–Sr isochron dates of 1066 ± 45 Ma (n = 60; biotite only) and 1050 ± 17 Ma (n = 63; biotite + apatite). These have been interpreted as the age of metamorphism and the age of thermal resetting or cooling related to the Musgrave Orogeny (Ribeiro et al., in prep.), respectively. An in situ monazite U–Pb date of 1557 ± 6 Ma (MSWD = 0.89) from this sample was interpreted as the age of metamorphism (GSWA 243071, preliminary data). Detrital zircon from a pelitic schist sample within the same drillcore yielded a conservative maximum deposition age of 1802 ± 7 Ma and zircon rims yielded an age of 1586 ± 8 Ma, interpreted as metamorphic (GSWA 243061, Wingate et al., 2022a). Detrital zircons from a quartzite about 8.8 km to the north yielded a conservative maximum depositional age of 1775 ± 7 Ma (GSWA 184341, Kirkland et al., 2009a). About 13.5 km to the west-southwest, a metagranodiorite of the Dwarf Well Granite, assigned to the 1779–1767 Ma Carrington Suite (Scrimgeour, 2013; Spaggiari and Kelsey, 2022), yielded an igneous crystallization age of 1773 ± 6 Ma (GSWA 184367, Kirkland et al., 2009b). About 13.5 km to the north-northeast, an altered granitic rock from drillcore EAL001 yielded an igneous crystallization age of 1608 ± 7 Ma and a metamorphic age, from non-zoned zircons, of 1577 ± 7 Ma (GSWA 203749, Wingate et al., 2022b).

Petrographic description

The sample is a pelitic schist containing 42% biotite, 27% quartz, 11% muscovite, 8% fibrolite and sillimanite, 6% magnetite, 4% garnet, 2% apatite and accessory plagioclase, chlorite, pyrite, monazite, zircon and xenotime (Figs 1, 2; Table 1). Biotite is coarse grained (up to 2–3 mm), straw-brown to brown–green in colour, stubby to acicular habit and defines a strong aggregated grain fabric. Well-developed, wide and dark radiation damage halos in biotite are common, caused by inclusions of monazite and zircon. The fabric is also defined by alternating foliae of biotite–fibrolite–muscovite and quartz–biotite–sillimanite±muscovite (Figs 2, 3). Quartz occurs as subhedral granoblastic grains (typically 0.5 – 1.0 mm

long) with curvilinear boundaries and internal subgrains. Muscovite is typically about the same size (about 2–3 mm long) as biotite but much more stubby in habit; and although its cleavage is commonly at a high angle to the biotite-rich fabric, the long axis of muscovite grains are commonly in the direction of the biotite fabric (Fig. 3). In this way, muscovite is part of the fabric. This coarse-grained muscovite contains inclusions of fibrolite, magnetite and quartz. Smaller grains of muscovite (about 0.5 – 1 mm long) occur at a high angle to the fabric and are interpreted as late (Fig. 3). Fibrolite is the dominant form of sillimanite, occurring as matted aggregates of needles on the margins of and among biotite aggregates in local patches in the sample, rather than distributed pervasively (Fig. 3). Matted aggregates of fibrolite needles also occur in quartz-rich regions and as inclusions in coarse-grained muscovite. Numerous grains of coarse-grained, prismatic sillimanite (about 0.1 – 3.0 mm) occur locally, some oriented parallel to the biotite fabric, others perpendicular. Garnet occurs as rounded–subhedral to anhedral poikiloblasts about 1–5 mm diameter with a low inclusion density. Inclusions in garnet are quartz, apatite, magnetite, and rare pyrite and sillimanite. The main fabric of the rock wraps around garnet but is also truncated by garnet. Magnetite is abundant and defines discontinuous layers parallel to, and helping to define, the main fabric, with grain size mostly ≤ 0.5 mm but up to 1 mm long. The grain shape of magnetite is euhedral to rounded and anhedral. The concentration of magnetite is higher in the strain shadows of garnet poikiloblasts. Apatite occurs throughout the sample as subangular to rounded grains that are commonly oriented with the main fabric. Chlorite (< 1 mm long) occurs as rare mantles on some biotite grains and is interpreted as late. Plagioclase (< 1 mm long) is rare and occurs mainly in the local region of the rock where coarse-grained sillimanite is present (Fig. 2) as anhedral grains in contact with biotite, quartz and sillimanite. This sample does not feature leucosomes.

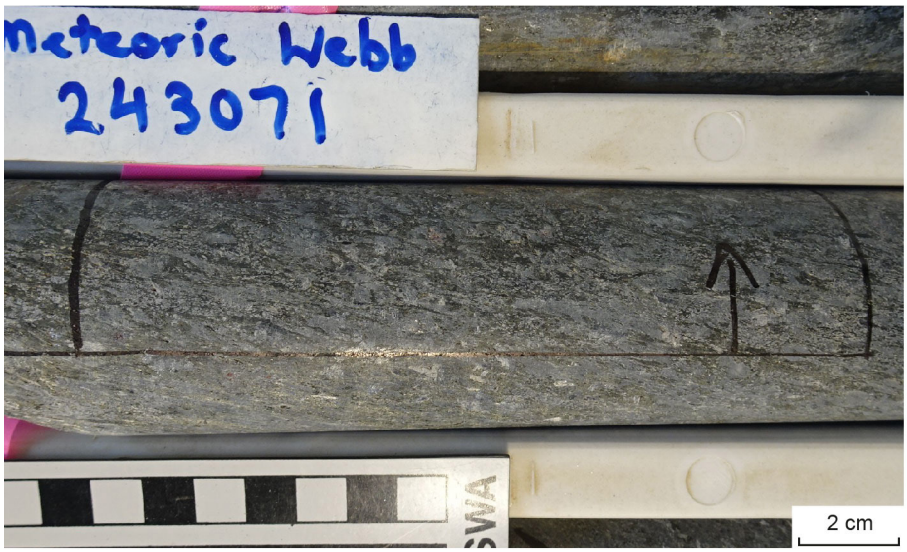

Figure 1. Drillcore image for sample 243071: garnet-bearing sillimanite–magnetite pelitic schist, Radiator prospect

Table 1. Mineral modes for sample 243071: garnet-bearing sillimanite–magnetite pelitic schist, Radiator prospect

Mineral modes	Bt	Qz	Ms	Sil [b]	Mag	Grt	Ap	Pl	Chl	Py
Observed (vol%)[a]	42	27	11	8	6	4	2	<1	<1	<1
Predicted (mol%)										
@ 625 °C, 3.4 kbar	40	28	9	16	3	<1	–	2	–	–
@ 675 °C, 6.5 kbar	36	27	15	13	3	3	–	<1	–	–

NOTES: (a) Trace monazite, zircon and xenotime also present in thin section
(b) In thin section, sillimanite is typically fibrolitic, intergrown with biotite
– not present

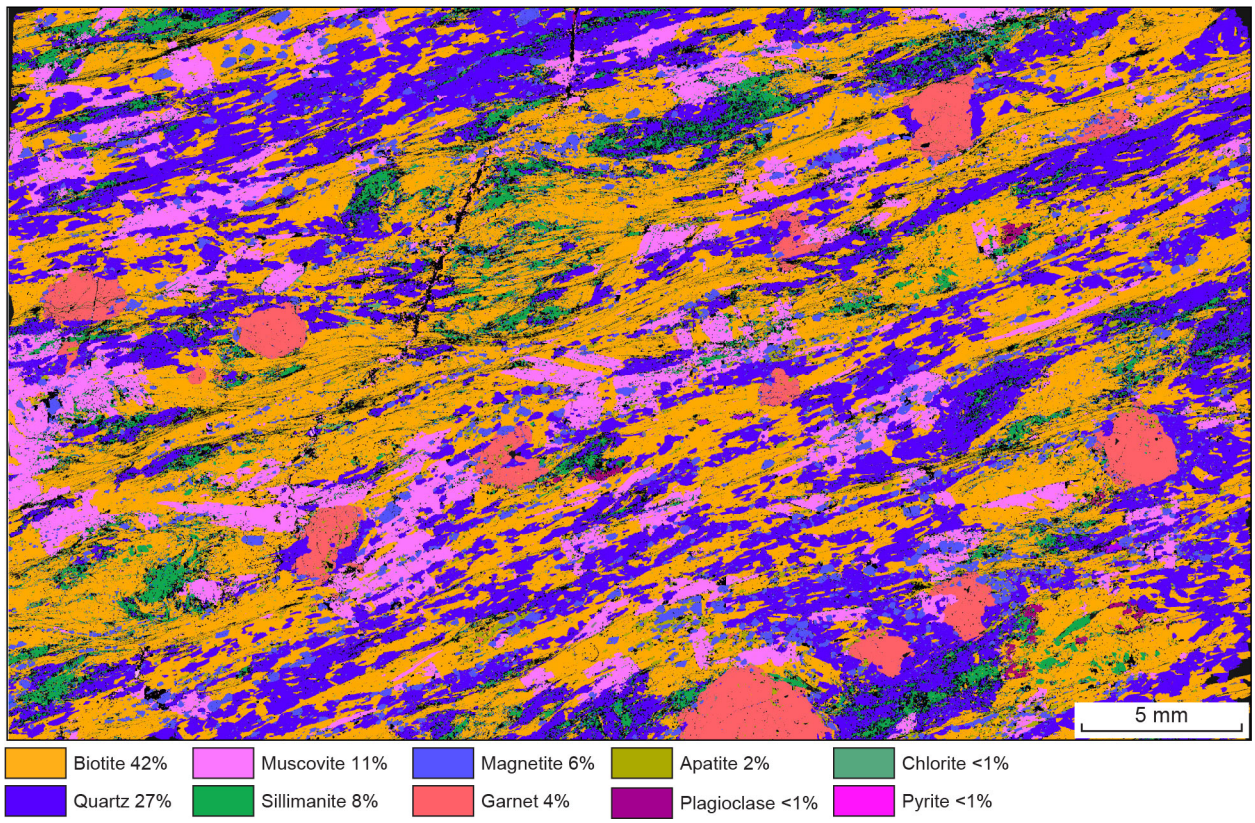

Figure 2. **TESCAN Integrated Mineral Analyser (TIMA) image of an entire thin section from sample 243071: garnet-bearing sillimanite–magnetite pelitic schist, Radiator prospect. Volume percent proportions of major rock-forming minerals are calculated by the TIMA software**

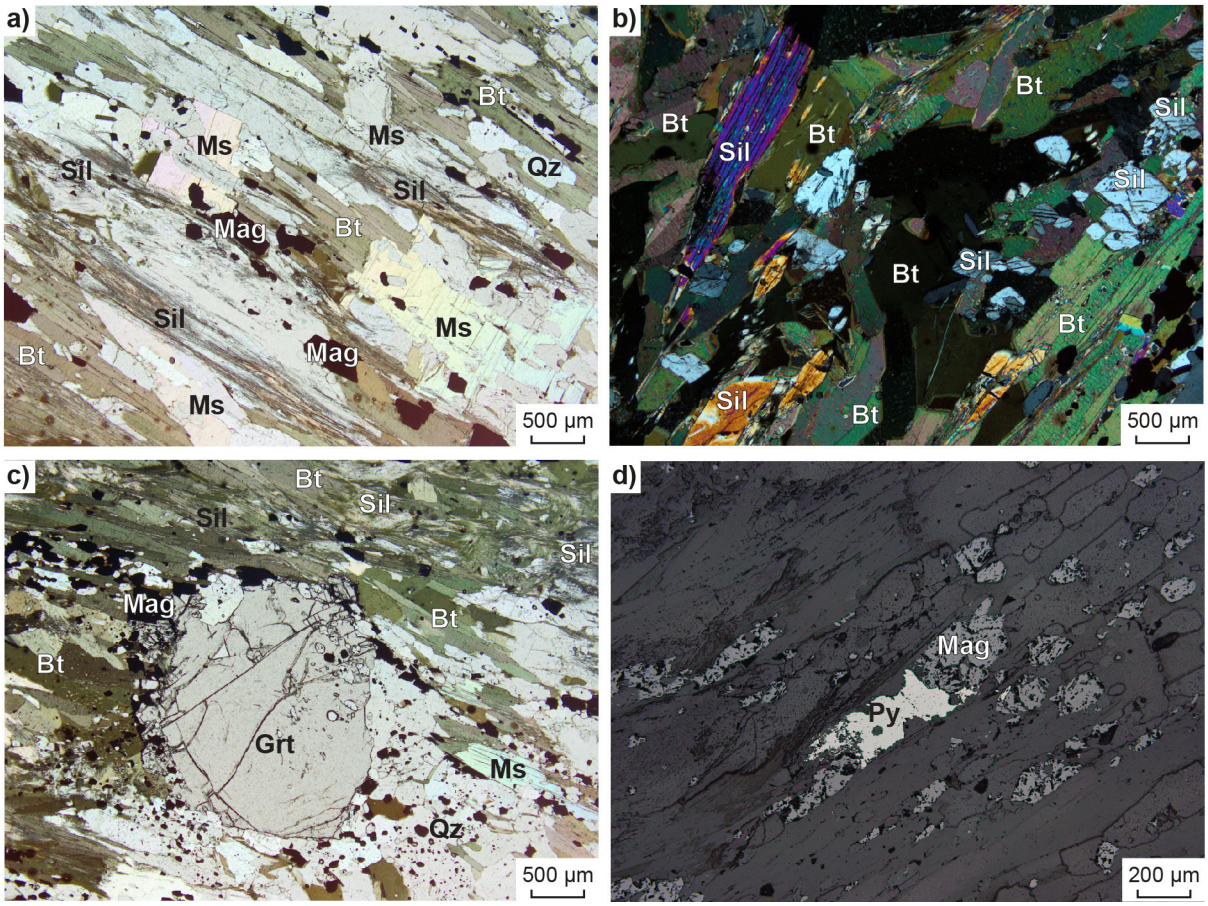

Figure 3. **Photomicrographs of sample 243071: garnet-bearing sillimanite–magnetite pelitic schist, Radiator prospect. Abbreviations: Bt, biotite; Grt, garnet; Mag, magnetite; Ms, muscovite; Py, pyrite; Qz, quartz; Sil, sillimanite**

Analytical details

The metamorphic evolution of this sample was investigated using phase equilibria, based on the bulk-rock composition (Table 2). The composition was determined by X-ray fluorescence spectroscopy, together with loss on ignition (LOI). FeO content was analysed by Fe^{2+} titration (as 76% of total Fe), and Fe_2O_3 calculated by difference. The modelled O content (for Fe^{3+}) was derived from the titration value. The H_2O content was based on the measured amount of LOI, corrected for oxidation state. The bulk composition was corrected for the presence of pyrite (sulfur) and apatite by applying a correction to iron and calcium, respectively (Table 2). Thermodynamic calculations were performed in the MnNCKFMASHTO ($MnO–Na_2O–CaO–K_2O–FeO–MgO–Al_2O_3–SiO_2–H_2O–TiO_2–O$) system using THERMOCALC version tc340 (updated October 2013; Powell and Holland, 1988) and the internally consistent thermodynamic dataset of Holland and Powell (2011; dataset tc-ds62, created in February 2012). The activity–composition relations used in the modelling are detailed in White et al. (2014a,b). Compositional and mode isopleths for all phases were calculated using the software TCInvestigator (Pearce et al., 2015; Appendix 2). Additional information on the workflow with relevant background and methodology are provided in Korhonen et al. (2020).

Mineral chemistry was acquired using a JEOL JXA-8530F Plus field emission electron microprobe (EPMA) at University of Tasmania, equipped with five wavelength-dispersive spectrometers. The EPMA is computer control by JEOL PC-EPMA and Probe Software Inc. 'Probe For EPMA' and 'Probe Image' software packages for all data acquisition and processing is used. Instrument operating conditions were 15 kV/10 nA with a 5 µm defocused beam. Matrix corrections of Armstrong-Love/Scott φ(ρz) (Armstrong, 1988) and Henke MACs were used for data reduction. Mean Atomic Number (MAN) background correction (e.g. Donovan and Tingle, 1996; Donovan et al., 2016) was used over traditional 2 point background interpolation. Well-characterized natural minerals were used as standards for microprobe analytical sessions. Mineral compositions are provided in Appendix 1 as an accompanying electronic file (see **Links**).

Table 2. Measured whole-rock and modelled compositions for sample 243071: garnet-bearing sillimanite–magnetite pelitic schist, Radiator prospect

XRF whole-rock composition (wt%)[a]												
SiO_2	**TiO_2**	**Al_2O_3**	**$Fe_2O_3^T$**	**FeO [b]**	**MnO**	**MgO**	**CaO**	**Na_2O**	**K_2O**	**P_2O_5**	**LOI**	**Total**
50.88	0.59	20.76	17.24	11.70	0.19	3.09	0.41	0.28	5.01	0.32	1.34	100.11
Normalized composition used for phase equilibria modelling (mol%)												
SiO_2	**TiO_2**	**Al_2O_3**	**O [c]**	**FeO^T [d]**	**MnO**	**MgO**	**CaO [e]**	**Na_2O**	**K_2O**	–	**H_2O [f]**	**Total**
53.49	0.46	12.86	1.65	13.61	0.16	4.84	0.01	0.29	3.36	–	9.25	100.00

NOTES: (a) Data and analytical details are available from the WACHEM database <http://geochem.dmp.wa.gov.au/geochem/>
(b) FeO content is by titration
(c) O content (for Fe_2O_3) set on basis of titrated FeO amount
(d) FeO^T = moles FeO + 2 * moles O. S from pyrite removed from FeO via FeO moles - 0.5*SO_2 moles
(e) CaO modified to remove apatite: CaO(Mod) = CaO(Total) - (moles CaO(in Ap) = 3.33 * moles P_2O_5)
(f) H_2O content is LOI adjusted for oxidation state

Results

Metamorphic *P–T* estimates have been derived based on detailed examination of one thin section and a single bulk-rock composition. Care was taken to ensure that the thin section and the sample volume selected for whole-rock chemistry were similar in terms of featuring the same minerals in about the same abundances (Table 1), to minimize any potential compositional differences. The *P–T* pseudosection for sample 243071 was calculated over a *P–T* range of 2–7 kbar and 525–700 °C (Fig. 4). The H_2O-saturated solidus has a minimum stability of 670 °C at 4.2 kbar over the modelled *P–T* range, and conditions above the solidus were not modelled due to the sample being subsolidus. Garnet is not stable in the high-temperature – low-pressure part of the modelled *P–T* range. Sillimanite is stable at temperatures above 580 °C in a wedge-shaped region expanding in pressure range to higher temperatures, with andalusite stable at lower pressures. At higher pressure, staurolite supersedes sillimanite stability. Muscovite is stable over most of the diagram, excepting a roughly triangular region in the low-pressure – high-temperature corner. Biotite and magnetite are stable everywhere across the modelled *P–T* range. Plagioclase is stable across the approximate *P–T* range 2.0 – 6.7 kbar and 525–725 °C. Chlorite is stable at lower than about 560 °C at 4.5 kbar and cordierite is stable below 3 kbar and >620 °C.

Garnet is weakly zoned and almandine rich (Appendix 3), with $Fe^{2+}/(Fe^{2+} + Mg + Mn + Ca)$ compositions higher at the rim (0.82) and lower (0.74 – 0.75) in the core (Appendix 1). Pyrope contents [$Mg/(Fe^{2+} + Mg + Mn + Ca)$] are low at the rim (0.05) and higher in the core (0.07 – 0.08). Spessartine contents [$Mn/(Fe^{2+} + Mg + Mn + Ca)$] are lower at the rim (down to 0.10) and higher in the core (0.16 – 017). Grossular contents [$Ca/(Fe^{2+} + Mg + Mn + Ca)$] are the same for rim and core (0.02). Biotite is Fe rich (XFe = $Fe^{2+}/(Fe^{2+} + Mg)$ = 0.65 – 0.67) and has TiO_2 wt% 1.23 – 1.62 (0.07 – 0.09 cations per formula unit [pfu]). Fluorine and chlorine ions in biotite are 0.07 – 0.07 and 0.00 pfu, respectively (11 oxygen basis). Muscovite has paragonite content of 0.12 – 0.14. Magnetite is pure and sillimanite contains 0.78 – 1.66 wt% FeO.

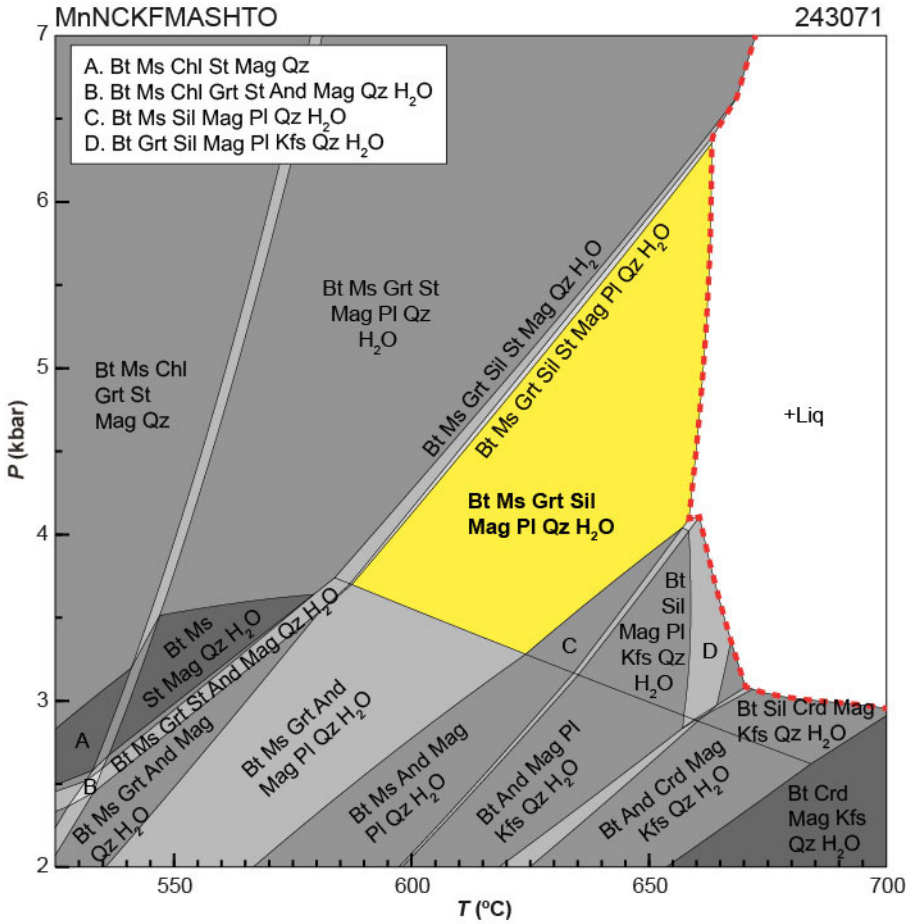

Figure 4. ***P–T*** **pseudosection calculated for sample 243071: garnet-bearing sillimanite–magnetite pelitic schist, Radiator prospect. Assemblage fields corresponding to peak metamorphic conditions are shown in bold text and yellow shading. Red dashed line represents the solidus. Abbreviations: And, andalusite; Bt, biotite; Chl, chlorite; Crd, cordierite; Grt, garnet; H_2O, aqueous fluid; Kfs, K-feldspar; Liq, silicate melt; Mag, magnetite; Ms, muscovite; Pl, plagioclase; Qz, quartz; Sil, sillimanite; St, staurolite**

Interpretation

The interpreted peak mineral assemblage of biotite–muscovite–garnet–sillimanite–magnetite–quartz±plagioclase is stable over the *P–T* range 3.3 – 6.3 kbar and 580–665 °C. The sample, and all schists in the drillcore, does not contain leucosomes and is therefore not partially melted, meaning that peak metamorphism did not reach the solidus. The absence of staurolite from the sample limits the maximum pressure for metamorphism. The lower pressure constraint is provided by the absence of andalusite from the sample, and the presence of garnet. Retrogression of the sample is limited to rare chlorite, though the occurrence of coarse-grained muscovite suggests it overprints the biotite fabric. Abundant apatite and magnetite in the sample suggest the schist has been affected by metasomatism/hydrothermal fluid flow;

and indeed potential IOCG style mineralization was one of the justifications for exploration drilling in the northern Aileron Province (Reddy, 2012). The apparent simplicity of the metamorphic parageneses is complicated by sample-specific and regional geochronological data. From the current sample, the Lu–Hf isochron age from garnet is distinctly older than zircon and monazite U–Pb dates for metamorphism from this sample and drillcore, though it is comparable to monazite U–Pb age data reported from the southern Aileron Province, at the Grapple prospect about 185 km to the southeast (Reno et al., 2018). The significance of this age difference is unclear at present, but may suggest there was either polymetamorphism or protracted metamorphism over the period 1670–1555 Ma. Long-lived metamorphism at this time driven by elevated crustal radiogenic heat production has been argued for the central Aileron Province (Alessio et al., 2020). Biotite Rb–Sr ages significantly younger than the garnet Lu–Hf and zircon U–Pb age data from the sample allow the possibility that either retrogression was temporally separate from the amphibolite facies metamorphism or that there is a record of exhumation related to the distal Musgrave Orogeny (e.g. Wong et al., 2015) that resulted in cooling below the closure temperature of biotite.

Peak metamorphic conditions are estimated at 3.3 – 6.3 kbar and 580–665 °C, with an apparent thermal gradient between 105 and 175 °C/kbar. There is limited petrological information to constrain any *P–T* path information

References

Alessio, KL, Hand, M, Hasterok, D, Morrissey, LJ, Kelsey, DE and Raimondo, T 2020, Thermal modelling of very long-lived (>140 Myr) high thermal gradient metamorphism as a result of radiogenic heating in the Reynolds Range, central Australia: Lithos, p. 352–353, doi:10.1016/j.lithos.2019.105280.

Armstrong, JT 1988, Quantitative analysis of silicates and oxide minerals: comparison of Monte-Carlo, ZAF and Phi-Rho-Z procedures *in* Proceedings of the Microbeam Analysis Society, *edited by* DE Newbury, San Francisco Press, San Francisco, p. 239.

Donovan, JJ and Tingle, TN 1996, An improved mean atomic number background correction for quantitative microanalysis: Journal of Microscopy and Microanalysis, v. 2, no. 1, p. 1–7.

Donovan, JJ, Singer, JW and Armstrong JT 2016, A new EPMA method for fast trace element analysis in simple matrices: American Mineralogist, v. 101, no. 8, p. 1839–1853.

Holland, TJB and Powell, R 2011, An improved and extended internally consistent thermodynamic dataset for phases of petrological interest, involving a new equation of state for solids: Journal of Metamorphic Geology, v. 29, no. 3, p. 333–383.

Hollis, JA, Kirkland, CL, Spaggiari, CV, Tyler, IM, Haines, PW, Wingate, MTD, Belousova, EA and Murphy, RC 2013, Zircon U-Pb-Hf isotope evidence for links between the Warumpi and Aileron Provinces, west Arunta region: Geological Survey of Western Australia, Record 2013/9, 30p.

Kelsey, DE, Spaggiari, CV, Wingate, MTD, Lu, Y, Fielding, IOH and Finch, EG 2021, Way out west – does the Arunta Orogen continue westward beneath the Canning Basin?: Australian Earth Sciences Convention, 9–12 February.

Kirkland, CL, Wingate, MTD, Spaggiari, CV and Tyler, IM 2009a, 184341: quartzite, Lake Mackay 818: Geological Survey of Western Australia, 5p.

Kirkland, CL, Wingate, MTD, Tyler, IM and Spaggiari, CV 2009b, 184367: metagranodiorite, Dwarf Well 846: Geological Survey of Western Australia, 4p.

Korhonen, FJ, Kelsey, DE, Fielding, IOH and Romano, SS 2020, The utility of the metamorphic rock record: constraining the pressure–temperature–time conditions of metamorphism: Geological Survey of Western Australia, Record 2020/14, 24p.

Pearce, MA, White, AJR and Gazley, MF 2015, TCInvestigator: automated calculation of mineral mode and composition contours for thermocalc pseudosections: Journal of Metamorphic Geology, v. 33, no. 4, p. 413–425, doi:10.1111/jmg.12126.

Powell, R and Holland, TJB 1988, An internally consistent dataset with uncertainties and correlations: 3. Applications to geobarometry, worked examples and a computer program: Journal of Metamorphic Geology, v. 6, no. 2, p. 173–204.

Reddy, D 2012, Surrender Report, Webb Project E80/3820 East Pilbara Shire, Western Australia, Reporting period 30 January 2008 to 12 June 2012: Geological Survey of Western Australia, Mineral Exploration Report A94934 (unpublished), 22p.

Reno, BL, McGloin, MV and Meffre, S 2018, Constraints on the timing of sulfide breccia formation at the Grapple Cu–Au–Ag–Zn prospect, central Australia: in situ LA–ICP–MS monazite geochronology of a new Proterozoic greenfields discovery: Northern Territory Geological Survey, Record 2018-013, 14p.

Ribeiro, BV, Kirkland, CL, Kelsey, DE, Reddy, S, Hartnday, MIH, Rankenburg, K, Liebmann, J, Korhonen, FJ and Clark, C in prep., In situ Rb–Sr reveals time–strain pathway for shear zone mylonitic fabrics: Earth and Planetary Science Letters.

Scrimgeour, IR 2013, Aileron Province: Chapter 12 *in* Geology and mineral resources of the Northern Territory, *compiled by* M Ahmad and TJ Munson, Northern Territory Geological Survey, Special Publication 5, p. 12:1 – 12:74.

Spaggiari, CV and Kelsey, DE (partial report), Dwarf Well Granite (P_-CNdw-mgm): Geological Survey of Western Australia, WA Geology Online, Explanatory Notes extract, viewed 7 July 2022, <www.dmirs.wa.gov.au/ens>.

White, RW, Powell, R, Holland, TJB, Johnson, TE and Green, ECR 2014a, New mineral activity-composition relations for thermodynamic calculations in metapelitic systems: Journal of Metamorphic Geology, v. 32, no. 3, p. 261–286.

White, RW, Powell, R and Johnson, TE 2014b, The effect of Mn on mineral stability in metapelites revisited: New a–x relations for manganese-bearing minerals: Journal of Metamorphic Geology, v. 32, no. 8, p. 809–828.

Wingate, MTD, Lu, Y, Fielding, IOH, Kelsey, DE and Spaggiari, CV 2022a, 243061: siliciclastic schist, Radiator prospect; Geochronology Record 1389: Geological Survey of Western Australia, 6p.

Wingate, MTD, Fielding, IOH and Lu, Y 2022b, 203749: altered granitic rock, Aileron prospect; Geochronology Record 1897: Geological Survey of Western Australia, 5p.

Wong, BL, Morrissey, LJ, Hand, M, Fields, CE and Kelsey, DE 2015 Grenvillian-aged reworking of late Palaeoproterozoic crust of the southern North Australian Craton, central Australia: Implications for the assembly of Mesoproterozoic Australia: Precambrian Research, v. 270, p. 100–123.

Appendix 2

Garnet compositional data from sample 243071: garnet-bearing sillimanite–magnetite pelitic schist, Radiator prospect, obtained by electron probe microanalyser (EPMA). Full compositional data provided in Appendix 1. $X(Fe^{2+}) = Fe^{2+}/(Fe^{2+} + Mg)$; $p(Alm) = Fe^{2+}/(Fe^{2+} + Mg + Ca + Mn)$; $p(Pyp) = Mg/(Fe^{2+} + Mg + Ca + Mn)$; $p(Grs) = Ca/(Fe^{2+} + Mg + Ca + Mn)$; $p(Sps) = Mn/(Fe^{2+} + Mg + Ca + Mn)$

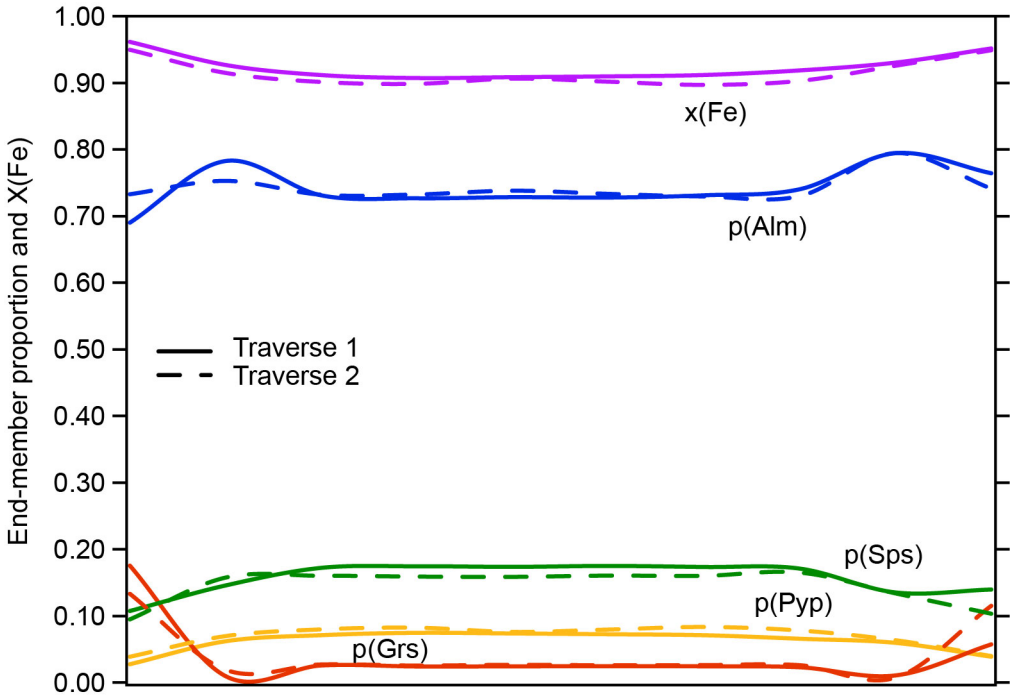

Appendix 3

Calculated phase volume percent modal proportion and solid-solution compositional data for sample 243071: garnet-bearing sillimanite–magnetite pelitic schist, Radiator prospect. Labelled *P–T* pseudosection shown in Figure 4. See Appendices 1 and 2 for definitions of compositional variables

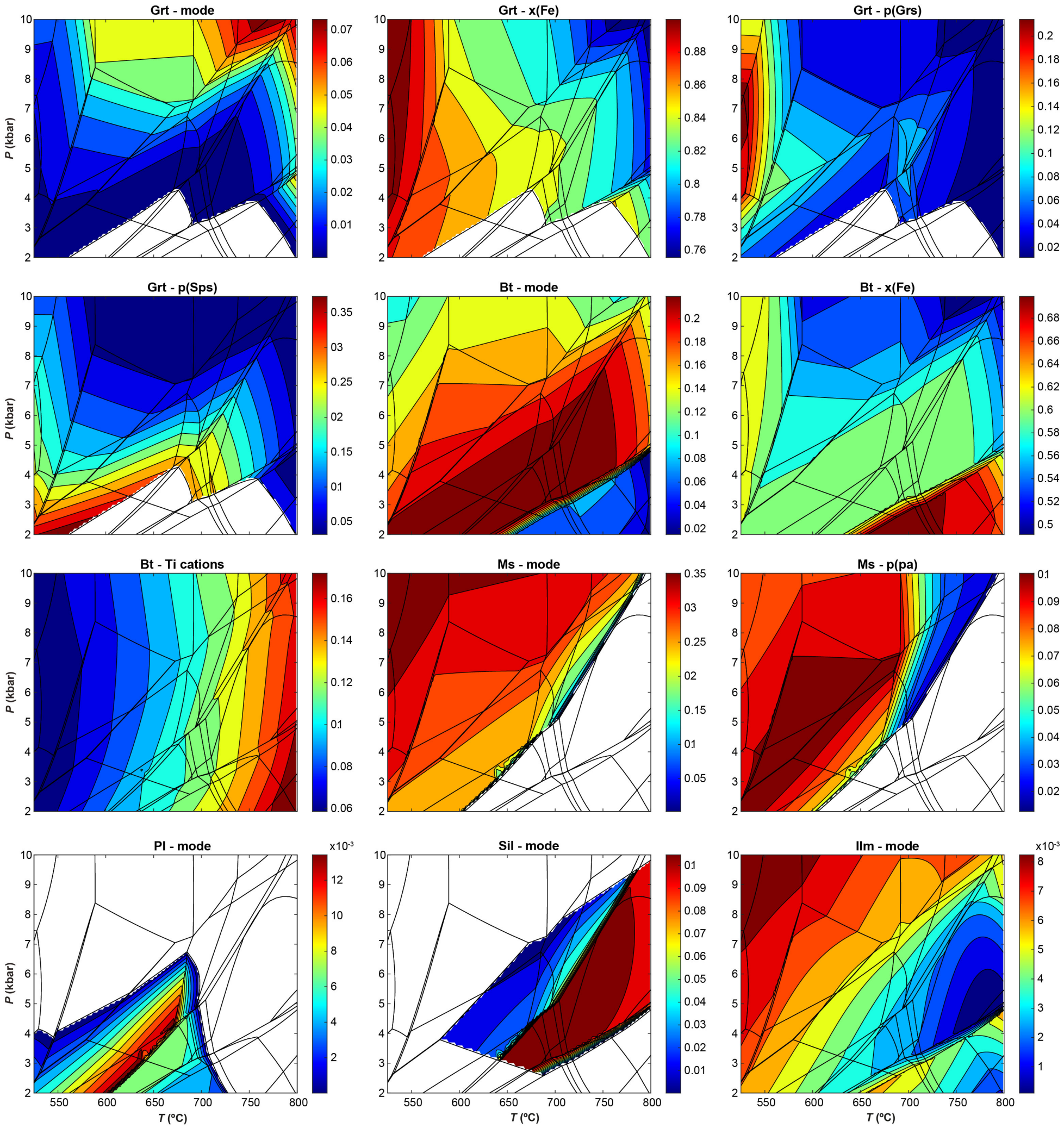

Links

Record 2020/14 The utility of the metamorphic rock record: constraining the pressure–temperature–time conditions of metamorphism

Appendix 1 (an accompanying electonic file on eBookshop)

Recommended reference for this publication

Kelsey, DE, Korhonen, FJ, Romano SS and Spaggiari, CV 2022, 243071: garnet-bearing sillimanite–magnetite pelitic schist, Radiator prospect; Metamorphic History Record 28: Geological Survey of Western Australia, 9p.

Data obtained: 22 August 2022

Date released: 9 December 2022

This Metamorphic History Record was last modified on 29 November 2022

Grid references in this publication refer to the Geocentric Datum of Australia 1994 (GDA94). All locations are quoted to at least the nearest 100 m.

WAROX is GSWA's field observation and sample database. WAROX site IDs have the format 'ABCXXXnnnnnnSS', where ABC = geologist username, XXX = project or map code, nnnnnn = 6 digit site number, and SS = optional alphabetic suffix (maximum 2 characters).

Isotope and element analyses are routinely conducted using the GeoHistory laser ablation ICP-MS and Sensitive High-Resolution Ion Microprobe (SHRIMP) ion microprobe facilities at the John de Laeter Centre (JdLC), Curtin University, with the financial support of the Australian Research Council and AuScope National Collaborative Research Infrastructure Strategy (NCRIS). The TESCAN Integrated Mineral Analyser (TIMA) instrument was funded by a grant from the Australian Research Council (LE140100150) and is operated by the JdLC with the support of the Geological Survey of Western Australia, The University of Western Australia (UWA) and Murdoch University. Mineral analyses are routinely obtained using the electron probe microanalyser (EPMA) facilities at the Centre for Microscopy, Characterisation and Analysis, UWA, at Adelaide Microscopy, University of Adelaide, and at the Electron Microscopy and X-ray Microanalysis Facility, University of Tasmania.

Digital data related to WA Geology Online, including geochronology and digital geology, are available online at the Department's Data and Software Centre and may be viewed in map context at GeoVIEW.WA.

Further details of geoscience products are available from:
Information Centre
Department of Mines, Industry Regulation and Safety
100 Plain Street
EAST PERTH WA 6004
Telephone: +61 8 9222 3459 | Email: publications@dmirs.wa.gov.au
www.dmirs.wa.gov.au/GSWApublications